Research Article Vol. 6, No. 10 | 1 Oct 2016 | OPTICAL MATERIALS EXPRESS 3354

Optical Materials EXPRESS

Effects of Zr^{4+} co-doping on the spectroscopic properties and yellow light emissions of Dy^{3+} in $LiNbO_3$ single crystals

S. W. LONG,[1,2] D. C. MA,[3] Y. Z. ZHU,[3] S. P. LIN,[3,4] AND B. WANG[1,2,3,5]

[1] *School of Physics, Sun Yat-sen University, Guangzhou 510275, China*
[2] *State Key Laboratory of Optoelectronic Materials and Technologies, Sun Yat-sen University, Guangzhou 510275, China*
[3] *Sino-French Institute of Nuclear Engineering and Technology, Sun Yat-sen University, Zhuhai 519082, China*
[4] *lshpeng@mail.sysu.edu.cn*
[5] *wangbiao@mail.sysu.edu.cn*

Abstract: A series of zirconium and dysprosium doped congruent $LiNbO_3$ (Zr:Dy:CLN) single crystals with a fixed concentration of Dy^{3+}(1mol%) and varied concentrations of optical damage resistant ion Zr^{4+} (0, 1, 2, 3mol%) have been grown successfully by the Czochralski technique. The influence of Zr^{4+} doping on structure and the spectroscopic characteristics of Dy^{3+} in Zr:Dy:CLN crystals have been investigated. Detailed Judd-Ofelt theory analysis was carried out to determine the Judd-Ofelt intensity parameters and main spectroscopic characteristics, which coincided well with the measured fluorescence performance. The defects, resulting from Li-deficiency or exceeding Zr^{4+}-doping, showed positive influences on the absorbing hypersensitive transition ${}^6H_{15/2} \to {}^6F_{11/2} + {}^6F_{9/2}$ and the parameter Ω_2. The stimulated emission cross sections of transition ${}^4F_{9/2} \to {}^6H_{13/2}$ with different Zr^{4+} concentration were evaluated. Exceeding Zr^{4+} doping was demonstrated effective for significantly eliminating the negative impact of threshold concentration on emission cross sections. The results showed a negative correlation between yellow fluorescence branching ratio of transition ${}^4F_{9/2} \to {}^6H_{13/2}$ and the symmetry of crystal field. Besides, we proposed the Zr:Dy:CLN single crystals as a candidate material for yellow laser operation.

© 2016 Optical Society of America

OCIS codes: (160.5690) Rare-earth-doped materials; (160.4760) Optical properties; (300.6280) Spectroscopy, fluorescence and luminescence; (160.3730) Lithium niobate.

References and links

1. Y. Liu, L. Liu, C. Zhou, and L. Xu, "Nonvolatile photorefractive holograms in $LiNbO_3$:CuCe crystals," Opt. Lett. **25**(12), 908–910 (2000).
2. T. Sakamoto, T. Kawanishi, and M. Izutsu, "Optoelectronic oscillator using a $LiNbO_3$ phase modulator for self-oscillating frequency comb generation," Opt. Lett. **31**(6), 811–813 (2006).
3. D. L. Zhang and E. Y. B. Pun, "Accurate measurement of 1.5 µm lifetime of Er^{3+} in $LiNbO_3$ crystals and waveguides," J. Appl. Phys. **94**(3), 1339–1346 (2003).
4. E. M. Rodríguez, D. Jaque, E. Cantelar, F. Cussó, G. Lifante, A. C. Busacca, A. Cino, and S. R. Sanseverino, "Time resolved confocal luminescence investigations on Reverse Proton Exchange Nd:$LiNbO_{(3)}$ channel waveguides," Opt. Express **15**(14), 8805–8811 (2007).
5. T. Tsuboi, S. M. Kaczmarek, Y. Nakai, and W. Huang, "The effect of Mg^{2+} ions in Er^{3+},Tm^{3+}-codoped $LiNbO_3$ single crystal," J. Lumin. **149**, 99–102 (2014).
6. M. Takahashi, K. Iyoda, T. Miyauchi, S. Ohkido, M. Tahashi, K. Wakita, N. Kajitani, M. Kurachi, and K. Hotta, "Preparation and characterization of Eu: Ti codoped $LiNbO_3$ films prepared by the sol-gel method," J. Appl. Phys. **106**(4), 44102 (2009).
7. I. Baumann, F. Cusso, B. Herreros, H. Holzbrecher, H. Paulus, K. Schafer, and W. Sohler, "Praseodymium-doped Ti:LiNbO3 waveguides," Appl. Phys., A Mater. Sci. Process. **68**(3), 321–324 (1999).
8. Y. F. Zheng, B. J. Chen, H. Y. Zhong, J. S. Sun, L. H. Cheng, X. P. Li, J. S. Zhang, Y. Tian, W. L. Lu, J. Wan, T. T. Yu, L. B. Huang, H. Q. Yu, and H. Lin, "Optical Transition, Excitation State Absorption, and Energy Transfer Study of Er^{3+}, Nd^{3+} Single-Doped, and Er^{3+}/Nd^{3+} Codoped Tellurite Glasses for Mid-Infrared Laser Applications," J. Am. Ceram. Soc. **94**(6), 1766–1772 (2011).

#274004 http://dx.doi.org/10.1364/OME.6.003354
Journal © 2016 Received 18 Aug 2016; revised 24 Sep 2016; accepted 26 Sep 2016; published 30 Sep 2016

9. Y. M. Yang, B. Q. Yao, B. J. Chen, C. Wang, G. Z. Ren, and X. J. Wang, “Judd-Ofelt analysis of spectroscopic properties of Tm^{3+}, Ho^{3+} doped GdVO4 crystals,” Opt. Mater. **29**(9), 1159–1165 (2007).
10. D. A. Turnbull, S. Q. Gu, and S. G. Bishop, “Photoluminescence studies of broadband excitation mechanisms for Dy^{3+} emission in Dy:$As_{12}Ge_{33}Se_{55}$ glass,” J. Appl. Phys. **80**(4), 2436–2441 (1996).
11. D. W. Hewak, B. N. Samson, J. A. M. Neto, R. I. Laming, and D. N. Payne, “Emission at 1.3µm from dysprosium-doped Ga:La:S glass,” Electron. Lett. **30**(12), 968–970 (1994).
12. Y. Wang, J. F. Li, Z. J. Zhu, Z. Y. You, J. L. Xu, and C. Y. Tu, “Mid-infrared emission in Dy:$YAlO_3$ crystal,” Opt. Mater. Express **4**(6), 1104–1111 (2014).
13. G. Dominiak-Dzik, W. Ryba-Romanowski, R. Lisiecki, P. Solarz, and M. Berkowski, “Dy-doped Lu_2SiO_5 single crystal: spectroscopic characteristics and luminescence dynamics,” Appl. Phys. B **99**(1–2), 285–297 (2009).
14. P. Haro-González, L. L. Martín, I. R. Martín, G. Grazyna Dominiak-Dzik, and W. Ryba-Romanowski, “Pump and probe measurements of optical amplification at 584nm in dysprosium doped lithium niobate crystal,” Opt. Mater. **33**(2), 196–199 (2010).
15. A. Lorenzo, E. Camarillo, H. S. Murrieta, E. Alvarez, U. G. Caldiño, J. A. Hernandez, M. Voda, F. Jaque, and J. Garcia Solé, “Optical spectroscopy of Dy^{3+} ions in $LiNbO_3$,” Opt. Mater. **5**(4), 251–258 (1996).
16. W. Ryba-Romanowski, G. Dominiak-Dzik, P. Solarz, and R. Lisiecki, “Transition intensities and excited state relaxation dynamics of Dy^{3+} in crystals and glasses: A comparative study,” Opt. Mater. **31**(11), 1547–1554 (2009).
17. G. Bolognesi, D. Parisi, D. Calonico, G. A. Costanzo, F. Levi, P. W. Metz, C. Kränkel, G. Huber, and M. Tonelli, “Yellow laser performance of Dy^{3+} in co-doped Dy,Tb:$LiLuF_4$,” Opt. Lett. **39**(23), 6628–6631 (2014).
18. Y. Tian, B. J. Chen, B. N. Tian, R. N. Hua, J. S. Sun, L. H. Cheng, H. Y. Zhong, X. P. Li, J. S. Zhang, Y. F. Zheng, T. T. Yu, L. B. Huang, and Q. Y. Meng, “Concentration-dependent luminescence and energy transfer of flower-like Y_2 $(MoO_4)_3$:Dy^{3+} phosphor,” J. Alloys Compd. **509**(20), 6096–6101 (2011).
19. X. H. Zhen, R. Wang, W. S. Xu, Y. H. Xu, and L. C. Zhao, “Study on photodamage of Mg: Ga: LiNbO3 crystal wave-guide substrate,” Opt. Mater. **19**(4), 427–431 (2002).
20. T. Volk, B. Maximov, T. Chernaya, N. Rubinina, M. Wohlecke, and V. Simonov, ““Photorefractive properties of $LiNbO_3$: Zn crystals related to the defect structure,” Appl. Phys. B-Lasers Opt. **72**(6), 647–652 (2001).
21. Y. N. Qian, R. Wang, C. Xu, W. Xu, X. H. Wu, and C. H. Yang, “Spectroscopic characteristics of 1.54µm emission in Er/Yb:$LiNbO_3$ crystals tridoped with In^{3+} ions,” J. Alloys Compd. **527**, 152–156 (2012).
22. S. Q. Fang, Y. J. Qiao, X. H. Zhang, and F. R. Ling, “Increased optical damage resistance in Ce: Cu: $LiNbO_3$ by doping with Sc_2O_3 for quasi-nonvolatile holographic storage,” Phys. Status Solidi A-Appl. Mat. **204**(3), 833–838 (2007).
23. T. Zhang, X. Wang, T. Geng, C. G. Tong, and C. Kang, “Enhanced photorefractive properties in Hf, Ce and Cu co-doped $LiNbO_3$ crystals for holographic application,” J. Alloys Compd. **629**, 255–259 (2015).
24. M. Abarkan, M. Aillerie, N. Kokanyan, C. Teyssandier, and E. Kokanyan, “Electro-optic and dielectric properties of Zirconium-doped congruent lithium-niobate crystals,” Opt. Mater. Express **4**(1), 179–189 (2014).
25. N. Argiolas, M. Bazzan, M. V. Ciampolillo, P. Pozzobon, C. Sada, L. Saoner, A. M. Zaltron, L. Bacci, P. Minzioni, G. Nava, J. Parravicini, W. Yan, I. Cristiani, and V. Degiorgio, “Structural and optical properties of zirconium doped lithium niobate crystals,” J. Appl. Phys. **108**(9), 093508 (2010).
26. Y. Kong, S. Liu, Y. Zhao, H. Liu, S. Chen, and J. Xu, “Highly optical damage resistant crystal: Zirconium-oxide-doped lithium niobate,” Appl. Phys. Lett. **91**(8), 081908 (2007).
27. B. R. Judd, “Optical Absorption Intensities of Rare-Earth Ions,” Phys. Rev. **127**(3), 750–761 (1962).
28. G. S. Ofelt, “Intensities of Crystal Spectra of Rare-Earth Ions,” J. Chem. Phys. **37**(3), 511–520 (1962).
29. D. H. Jundt, “Temperature-dependent Sellmeier equation for the index of refraction, n(e), in congruent lithium niobate,” Opt. Lett. **22**(20), 1553–1555 (1997).
30. G. Nava, P. Minzioni, W. B. Yan, J. Parravicini, D. Grando, E. Musso, I. Cristiani, N. Argiolas, M. Bazzan, M. V. Ciampolillo, A. Zaltron, C. Sada, and V. Degiorgio, “Zirconium-doped lithium niobate: photorefractive and electro-optical properties as a function of dopant concentration,” Opt. Mater. Express **1**(2), 270–277 (2011).
31. W. T. Carnall, “Electronic Energy Levels in the Trivalent Lanthanide Aquo Ions. I. Pr3+, Nd3+, Pm3+, Sm3+, Dy^{3+}, Ho^{3+}, Er^{3+}, and Tm^{3+},” J. Chem. Phys. **49**(10), 4424 (1968).
32. C. K. Jayasankar and E. Rukmini, “Spectroscopic investigations of Dy^{3+} ions in borosulphate glasses,” Physica B **240**(3), 273–288 (1997).
33. P. Lerner, C. Legras, and J. P. Dumas, “Stoechiométrie des monocristaux de métaniobate de lithium,” J. Cryst. Growth **3–4**, 231–235 (1968).
34. Z. H. Tang, S. P. Lin, D. C. Ma, and B. Wang, “Blue and green upconversion emissions of Zr: Nd: $LiNbO_3$ single crystals,” Int. J. Mod. Phys. B **29**(13), 1550080 (2015).
35. Y. Z. Zhu, S. P. Lin, Y. Zheng, D. C. Ma, and B. Wang, “Improvement of pyroelectric figures of merit in zirconia-doped congruent lithium niobate single crystals,” J. Mater. Sci. **51**(6), 3155–3161 (2016).
36. C. Xu, C. H. Yang, L. Dai, L. A. Sun, Y. H. Xu, and L. C. Cao, “Influence of Li and Nb ratios on the defect structure and exposure energy in $LiNbO_3$:Fe:Mn:Zr crystals,” J. Alloys Compd. **509**(10), 4167–4170 (2011).
37. L. Dai, C. Xu, Z. Qian, J. Li, D. Y. Li, and Y. H. Xu, “Influence of In^{3+} ions concentration on the defect structure and light-induced scattering of Ce:Mn:$LiNbO_3$ crystals,” J. Lumin. **134**, 255–259 (2013).
38. K. Polgár, Á. Péter, L. Kovács, G. Corradi, and Z. Szaller, “Growth of stoichiometric $LiNbO_3$ single crystals by top seeded solution growth method,” J. Cryst. Growth **177**(3–4), 211–216 (1997).

39. B. Zhou, E. Y.-B. Pun, H. Lin, D. Yang, and L. Huang, "Judd–Ofelt analysis, frequency upconversion, and infrared photoluminescence of Ho^{3+} -doped and Ho^{3+} /Yb^{3+} -codoped lead bismuth gallate oxide glasses," J. Appl. Phys. **106**(10), 103105 (2009).
40. M. D. Shinn, W. A. Sibley, M. G. Drexhage, and R. N. Brown, "Optical transitions of Er^{3+} ions in fluorozirconate glass," Phys. Rev. B Condens. Matter **27**(11), 6635–6648 (1983).
41. G. Dominiak-Dzik, W. Ryba-Romanowski, M. N. Palatnikov, N. V. Sidorov, and V. T. Kalinnikov, "Dysprosium-doped $LiNbO_3$ crystal. Optical properties and effect of temperature on fluorescence dynamics," J. Mol. Struct. **704**(1–3), 139–144 (2004).
42. B. R. Judd, "Hypersensitive Transitions in Rare-Earth Ions," J. Chem. Phys. **44**(2), 839–840 (1966).
43. S. F. Mason, R. D. Peacock, and B. Stewart, "Ligand-polarization contributions to the intensity of hypersensitive trivalent lanthanide transitions," Mol. Phys. **30**(6), 1829–1841 (1975).
44. G. Malovichko, V. Grachev, E. Kokanyan, and O. Schirmer, "Axial and low-symmetry centers of trivalent impurities in lithium niobate: Chromium in congruent and stoichiometric crystals," Phys. Rev. B **59**(14), 9113–9125 (1999).
45. P. A. Ryabochkina, S. A. Antoshkina, E. V. Bolshakova, M. A. Ivanov, V. V. Kochurihin, A. V. Malov, S. N. Ushakov, N. V. Shchuchkina, and K. N. Nishchev, "Hypersensitive transitions of Tm^{3+}, Ho^{3+} and Dy^{3+} rare-earth ions in garnet crystals," J. Lumin. **132**(8), 1900–1905 (2012).
46. A. H. Li, Q. Lu, Z. R. Zheng, L. Sun, W. Z. Wu, W. L. Liu, Y. Q. Yang, and T. Q. Lu, "Yellow-green upconversion luminescence of Dy^{3+} ion in $LiNbO_3$ crystal heavily codoped with ZnO," J. Appl. Phys. **102**(11), 113102 (2007).
47. J. A. Caird, L. G. DeShazer, and J. Nella, "Characteristics of room-temperature 2.3-μm laser emission from tm^{3+}in YAG and YAlO3," IEEE J. Quantum Electron. **11**(11), 874–881 (1975).

1. Introduction

Lithium niobate (LN) is one of the most widely used integrated optical materials thanks to the excellent electro-optical and nonlinear optics properties. There are extensive applications of this material in holographic storage [1] and optoelectronic devices [2]. With the high optical transparency from 350nm to 1800nm, Lithium niobate could work as a promising solid state lasing material at the visible and infrared wavelength range, when co-doped with trivalent lanthanide rare earth ions. Therefore, Considerable researches on spectroscopy and level structure of a variety of rare earth ions (such as Er^{3+}, Nd^{3+}, Tm^{3+}, Eu^{3+} and Pr^{3+}) in LN have been carried out for deeper insight into the laser system with high efficiency [3–9].

Compared to the rare earth ions mentioned above, far less work had been focused on the Dy^{3+} doped solid state materials. Earlier researches on Dy^{3+} doped solid state materials were concentrated in near-infrared (1.3 1.55 [10] and 1.7μm [11]) and mid-infrared (3μm [12]) emissions. Despite several current successful approaches to generate yellow laser, absence of appropriate active medium still restricted the development of all new compact solid state yellow laser source which could be pumped with commercially accessible operation wavelength. As a consequence, with the efficient energy level transition of Dy^{3+} from $^4F_{9/2}$ to $^6H_{13/2}$, researchers recently have been more inclined to study the potential of Dy^{3+} operating as yellow luminescence center [13–18].

In both scientific research and commercial application, congruent $LiNbO_3$ (CLN) (molar ratio [Li]/[Nb] = 0.946) is preferred than the near stoichiometric $LiNbO_3$ (SLN) because of the better uniformity and easier accessibility. Nevertheless, due to intrinsic defects resulting from deviation of Li-Nb ratio and Li-deficiency, CLN has relatively low optical damage resistance when exposed to high laser intensity, which severely limits the performance of Dy:CLN. One effective approach to suppress optical damage, which attracts many researchers' interest, consists in co-doping with optical damage resistant ions, such as Mg^{2+}, Zn^{2+}, In^{3+}, Sc^{3+}, Hf^{4+} and Zr^{4+} [19–24]. Among all the optical damage resistant ions, tetravalent Zr^{4+} presents the lowest threshold concentration of 2mol% and a distribution coefficient closer to one [25, 26], guaranteeing the quality of optical crystals. It is therefore of interest to know the spectroscopic and structural properties of Dy:CLN after co-doping with Zr^{4+}.

In the present work, the effects of Zr^{4+} co-doping on the yellow light emissions of Dy^{3+} in LN single crystals have been extensively studied by preparing a series of Zr:Dy:CLN single crystals with the Czochralski technique. Based on X-ray diffraction patterns and UV absorption spectra, a brief location analysis of Zr^{4+} was given. Detailed Judd-Ofelt theory analysis was carried out to study the influence of Zr^{4+} co-doping on the spectroscopic properties of Dy^{3+} in $LiNbO_3$ single crystals. Besides, with the analysis of the measured fluorescence characteristics, the relation between yellow luminescence emissions and structure transmutation in Dy^{3+} and Zr^{4+} co-doped CLN crystals were discussed.

2. The Judd-Ofelt theory

The Judd-Ofelt theory (J-O theory) was put forward by Judd [27] and Ofelt [28] separately in 1962. This theory is the most effective way to study *4f-4f* transition of rare earth ions in crystal field, with which spectral intensity parameters of rare earth ions in a variety of host materials have been calculated and analyzed. There are some important formulas as follows:

The experimental oscillator strength for transition from ground state to excited state:

$$f_{\exp} = \frac{mc^2}{N\pi\bar{\lambda}^2 e^2}\int \alpha(\lambda)d\lambda; \tag{1}$$

where $\bar{\lambda}$ is mean wavelength of absorption band; N is the doping concentration of dopant in crystals, such as Dy^{3+}; m and e are the mass and charge of electron respectively; c is the velocity of light; $\alpha(\lambda)$ is the absorption coefficient, the integration of which can be figured out according to the UV-Vis-NIR absorption spectroscopy.

The oscillator strength for electric dipole transition from state $4f^N J$ to $4f^N J'$:

$$f_{ed} = \frac{8\pi^2 mc}{3h(2J+1)\bar{\lambda}}\frac{(n^2+2)^2}{9n}\sum\nolimits_{\delta=2,4,6}\Omega_\delta \left\langle 4f^N\varphi J \,\|\, U^\delta \,\|\, 4f^N\varphi' J'\right\rangle^2; \tag{2}$$

where h is Planck constant; n is refractive index, the values of which were obtained in the [29, 30]; Ω_δ are the oscillator strength parameters; δ is only 2, 4 or 6 which is resulted from the transition selection rule of electric dipole; $\left\langle 4f^N\varphi J \left\| U^\delta \right\| 4f^N\varphi' J'\right\rangle$, which is inert to crystal field, are reduced matrix elements of unit tensor operators U^δ. They were cited from [31]. and [32]. to make calculation of oscillator strength parameters Ω_δ and fluorescence branching ratios respectively.

The oscillator strength for magnetic dipole transition from state $4f^N J$ to $4f^N J'$:

$$f_{md} = \frac{nh}{6mc(2J+1)\bar{\lambda}}\left\langle 4f^N\varphi J \left\| L+2S \right\| 4f^N\varphi' J'\right\rangle^2; \tag{3}$$

where $\left\langle 4f^N\varphi J \left\| L+2S \right\| 4f^N\varphi' J'\right\rangle$ is the reduced matrix element of magnetic dipole operator $L + 2S$. For the transitions $^4F_{9/2} \rightarrow {}^6F_{7/2}$, $^4F_{9/2} \rightarrow {}^6H_{7/2}$, $^4F_{9/2} \rightarrow {}^6F_{9/2}$, $^4F_{9/2} \rightarrow {}^6H_{9/2}$, $^4F_{9/2} \rightarrow {}^6F_{11/2}$ and $^4F_{9/2} \rightarrow {}^6H_{11/2}$ of Dy^{3+} ions, magnetic-dipole component makes a significant contribution and should be taken into account.

For Dy^{3+}, transition of electric dipole and magnetic dipole dominate the *4f-4f* transition:

$$f_{cal} \approx f_{\exp} = f_{md} + f_{ed}; \tag{4}$$

According with other formulas above, oscillator strength parameters Ω_δ would be computed by least square method and then used to calculate f_{cal}.

The root mean square deviation of fitting is defined as:

$$\Delta f_{rms} = \sqrt{\frac{\sum_{i=1}^{Num}(f_{cal} - f_{\exp})^2}{Num-3}}; \tag{5}$$

where Num is the number of absorption bands involved in calculation.

Transition probability of electric dipole (A_{ed}), magnetic dipole (A_{md}) and total *4f-4f* (A):

$$A = A_{ed} + A_{md} = \frac{8\pi^2 e^2 n^2}{mc\overline{\lambda}^2} f_{ed} + \frac{8\pi^2 e^2 n^2}{mc\overline{\lambda}^2} f_{md}; \tag{6}$$

The radiant lifetime τ of excited level i:

$$\tau_i = \frac{1}{\sum_k A_{ik}} \quad (i->k); \tag{7}$$

where A_{ik} is the radiative transition probability from level i to level k.

The fluorescence branching ratios β for transitions originating from level i:

$$\beta_{ik} = A_{ik}\tau_i \quad (i->k); \tag{8}$$

3. Experimental

CLN crystals of good quality with fixed Dy^{3+} concentration (1mol%) and varied Zr^{4+} concentration (0mol%, 1mol%, 2mol%, 3mol%) have been grown along the *c* axis from congruent melt (molar ratio [Li]/[Nb] = 0.946) by using the Czochralski method. The Homogeneous single crystal Zr(1mol%):Dy(1mol%):CLN, showing typical appearance of Zr:Dy:CLN crystals, was showed in Fig. 1(a). Wafers oriented perpendicular to *c* axis with the thickness of 2.5mm were cut from the central part of crystals and polished for further optical analysis, as shown in Fig. 1(b). The sample wafers with Zr-doped concentration from 0mol% to 3mol% were referred as Zr-0, Zr-1, Zr-2 and Zr-3 respectively thereinafter.

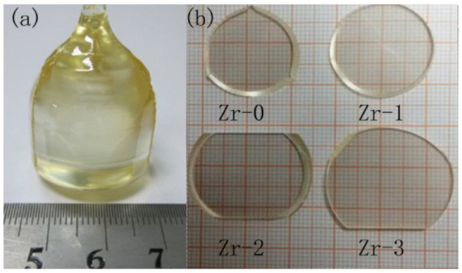

Fig. 1. (a) The as-grown single crystal of Zr(1mol%):Dy(1mol%):CLN with a diameter of 25 mm approximately, displaying the typical appearance of Zr:Dy:CLN crystals. (b) The polished Zr:Dy:CLN wafers oriented perpendicular to *c* axis with different Zr^{4+} concentration from 0mol% to 3mol%.

The polarized absorption spectra of the wafers (spanning wavelengths from 350 to 2000nm) and the ultraviolet absorption spectra were recorded using a Lambda 950 UV-Vis-NIR Spectrophotometer at room temperature. Prior to the measurement of polarized absorption spectra, except for the wafers Zr-0~3 oriented perpendicular to *c* axis mentioned above, the wafers oriented parallel to *c* axis had been also obtained from the same crystals.

The fluorescence emission spectra were acquired using an EDINBURGH FLSP980 Photoluminescence Spectrometer. Fluorescence lifetime decay curves were measured with an EDINBURGH FLSP920 spectrometer pumped by a μF900 flash lamp.

X-ray diffraction patterns from 20deg to 80deg were measured by a D-MAX 2200 VPC X-Ray Diffractometer.

4. Results and discussion

4.1 Location analysis of doping ions and shift of absorption edge

$LiNbO_3$ has a trigonal crystal structure with the space group *R3c* and the point group *3m* at room temperature. As a consequence of Li-deficiency in CLN, Nb^{5+} will enter Li-vacancy and exist in the form of $\mathrm{Nb}_{\mathrm{Li}}^{4+}$ [33]. The XRD patterns of CLN (JCPDS 78-0251) and Zr:Dy:CLN crystals were showed in Fig. 2(a). The diffraction peaks attributed to CLN were marked with the indices of the corresponding crystallographic planes. There was no new diffraction peak in the XRD patterns of all the samples, which indicated no remarkable change in the lattice structure after doping with Dy^{3+} and Zr^{4+}. Dy^{3+} would be located at Li^{+} site or Nb^{5+} site after Zr^{4+} entered the lattice. According to the Li vacancy defect model of CLN [33], damage resistant ion Zr^{4+} enters into the lattice in 2 different forms in sequence: firstly replacing $\mathrm{Nb}_{\mathrm{Li}}^{4+}$, then replacing Li^{+} after reaching the thresholds. Below the threshold concentration of Zr^{4+}, Zr^{4+} would substitute $\mathrm{Nb}_{\mathrm{Li}}^{4+}$ in the form of $\mathrm{Zr}_{\mathrm{Li}}^{3+}$, repelling $\mathrm{Nb}_{\mathrm{Li}}^{4+}$ and reducing the vacancies $\mathrm{V}_{\mathrm{Li}}^{-}$, followed by evidently increasing of the unit cell volume on account of the lower polarization ability of Zr^{4+} than that of Nb^{5+} [34, 35]. This increase would stop when Zr^{4+} substituted normal Li^{+} in Li site with a minor increase of Li vacancies after threshold achieved. Lattice parameters and cell volumes of Zr:Dy:CLN crystals were calculated by least square method. The unit cell volumes plotted in Fig. 2(b) agreed well with the model above.

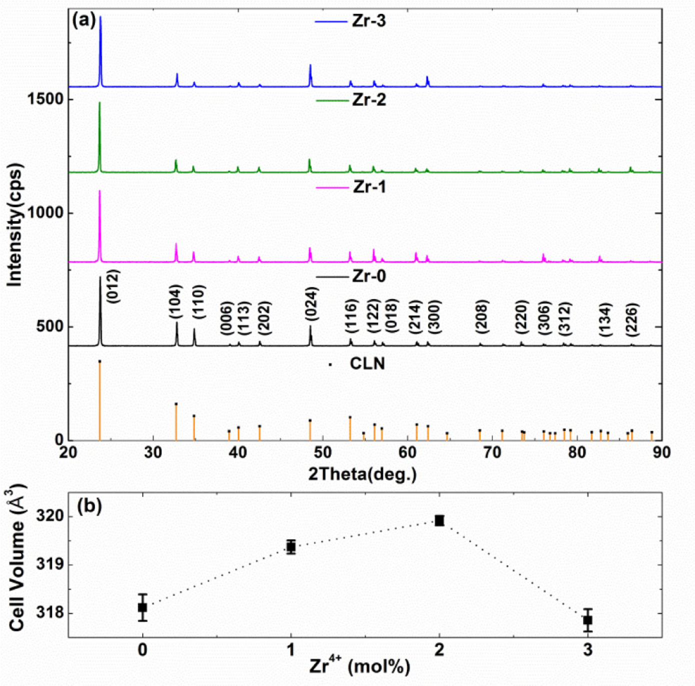

Fig. 2. (a) X-ray powder diffraction patterns of CLN (JCPDS 78-0251) and Zr:Dy:CLN polycrystalline powders which were obtained from the as-grown Zr:Dy:CLN crystals. (b) The cell volumes of Zr:Dy:CLN crystals with fixed concentrations of Dy^{3+} (1mol%) and different concentrations of Zr^{4+}.

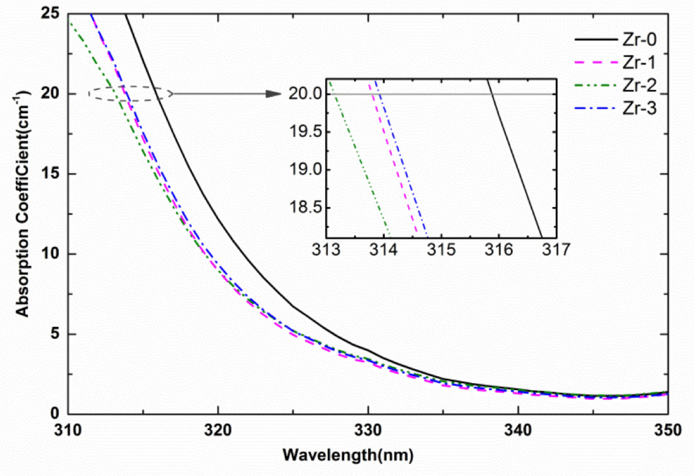

Fig. 3. Ultraviolet absorption spectra of Zr:Dy:CLN crystals from 310nm to 350nm at room temperature. The inset is the partial enlarged figure, showing the absorption edge positions.

The absorption edge position, which is an important reflection to structure and defects of CLN, is defined as the UV wavelength position where absorption coefficient $\alpha(\lambda)$ is equal to 20 cm^{-1}. As showed in Fig. 3 and the inset, there were first violet shifts from 315.88nm to 313.80nm and from 313.80nm to 313.14nm for the absorption edge, followed by a red shift from 313.14nm to 313.93nm. The Zr^{4+} concentration had reached the threshold at 2mol%, which corresponded to the minimum of absorption edge position [24]. The Zr^{4+} threshold concentration can be explained with the change of valence electron transition energy from 2p orbits of O^{2-} to 4d orbits of Nb^{5+}, which directly affects the absorption edge position [35–37]: Replacement with ions of higher (lower) polarizability would increasing (decreasing) polarization ability of O^{2-} and decreasing (increasing) the energy gap, resulting in a red (violet) shift of the absorption edge. Therefore, since the polarizability of Nb^{5+} was much stronger than Li^+, the energy gap would be decreased to cause a red shift in CLN deviating from 303nm [38] of stoichiometric $LiNbO_3$ (SLN). When Nb_{Li}^{4+} was replaced by Zr^{4+}, the polarizability of which is between Li^+ and Nb^{5+} ($Li^+ < Zr^{4+} < Nb^{5+}$), there would be a violet shift for the absorption edge but not reaching 303nm. After reaching the threshold concentration of Zr^{4+}, all Nb_{Li}^{4+} had been substituted. Additional Zr^{4+} would substitute Li^+, with red shift dominating. Hence, with the minimum wavelength value of absorption edge, we drew the inference that Nb_{Li}^{4+} had been replaced completely and the covalent bonding closest to SLN had been formed at 2mol% Zr^{4+} threshold concentration [38].

4.2 Optical properties and Judd-Ofelt analysis

The UV-VIS-NIR absorption spectra, measured in the 350-2000nm wavelength range at room temperature, were presented in Fig. 4. Seven absorption bands in the UV-Vis-NIR absorption spectra related to transitions of Dy^{3+} from ground state $^6H_{15/2}$ to excited states ^6H and ^6F terms were marked up. Significant absorption line broadening could be observed.

Besides electric dipole transitions, magnetic dipole transitions should be taken into account for $^6H_{15/2}\rightarrow{}^4I_{15/2}$ transition of Dy^{3+}. For simplicity, we chose the six absorption bands at longer wavelength region for J-O analysis mentioned above. f_{exp}, f_{cal} and Δf_{rms} were derived and listed in Table 1. Since the oscillator strength parameters Ω_δ, introduced to give a good fit with the experimental data by Judd [27], are important structure and laser characteristics: Ω_2 often plays only a minor role in determining the oscillator strengths [27] but is sensitive to the symmetry and the covalent bonding of the RE sites. The ratio Ω_4/Ω_6 allows for a prediction of the stimulated emission probability [39, 40]. The oscillator strength parameters Ω_δ and quality factor $X = \Omega_4/\Omega_6$ of Dy^{3+} and Zr^{4+} co-doped CLN were derived and presented in Table 2. The J-O analysis results of Zr-0 were consistent with those reported in [41]. The differences could be explained with the Li-deficiency in CLN, different concentration of Dy^{3+} and different test environments.

Table 1. Measured and calculated oscillator strengths, root mean square deviation of Zr:Dy:CLN crystals.

	Zr-0			Zr-1			Zr-2			Zr-3		
Transition	The oscillator strength f (10^{-6})											
$^6H_{15/2}\rightarrow$	f_{exp}	f_{cal}	Δf_{rms}	f_{exp}	f_{cal}	Δf_{rms}	f_{exp}	f_{cal}	Δf_{rms}	f_{exp}	f_{cal}	Δf_{rms}
$^4I_{15/2}$	0.79	0.88	0.32	0.76	0.86	0.33	0.69	0.83	0.27	0.74	0.85	0.28
$^6F_{3/2}$	0.36	0.29		0.36	0.28		0.35	0.28		0.36	0.28	
$^6F_{5/2}$	1.95	1.55		1.96	1.48		1.90	1.45		1.92	1.48	
$^6F_{7/2}$	3.48	3.21		3.32	3.10		2.99	2.96		3.13	3.04	
$^6H_{7/2}$+$^6F_{9/2}$	3.65	3.73		3.60	3.67		3.29	3.31		3.41	3.44	
$^6H_{9/2}$+$^6F_{11/2}$	9.12	9.09		9.16	9.13		8.20	8.18		8.76	8.74	
$^6H_{11/2}$	1.63	1.85		1.59	1.79		1.60	1.72		1.63	1.78	

Measured oscillator strengths were determined with polarized oscillator strengths: $f_{exp} = (f_\pi + 2f_\sigma)/3$).

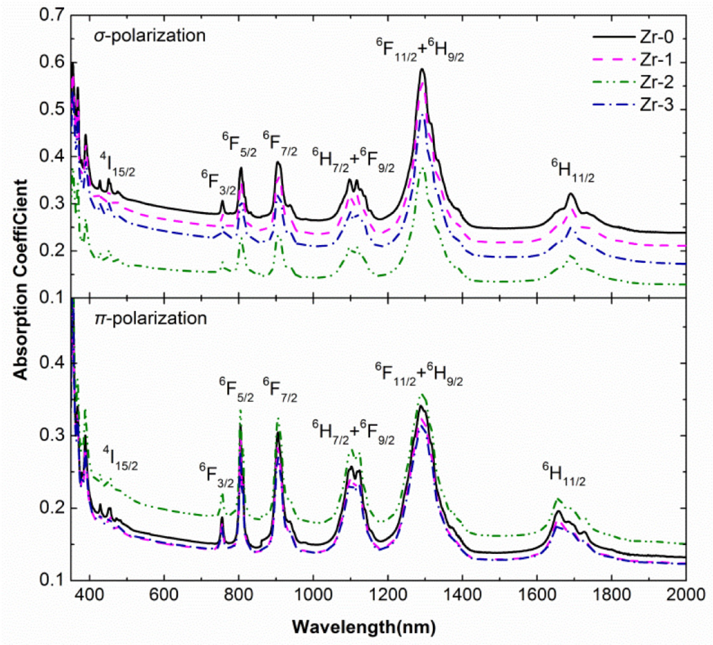

Fig. 4. The polarized absorption spectra of Zr:Dy:CLN crystals from 350nm to 2000nm at room temperature.

Table2. The oscillator strength parameters Ω_δ and quality factors X of Zr:Dy:CLN crystals.

Crystal	Ω_2(10^{-20}cm^2)	Ω_4(10^{-20}cm^2)	Ω_6(10^{-20}cm^2)	X (Ω_4/Ω_6)
Zr-0	5.52	1.53	2.20	0.69
Zr-1	5.56	1.58	2.12	0.75
Zr-2	5.09	1.21	2.08	0.58
Zr-3	5.45	1.31	2.11	0.62

As showed in Table 2, Ω_6 was insensitive to the transmutation of crystal structure which was resulted from different Zr^{4+} concentrations. The minimum of Ω_4 occurred at threshold concentration of Zr^{4+}. Then the value of Ω_4 recovered to 1.31 with the concentration of Zr^{4+}

exceeding up to 3mol%. The quality factors presented a similar trend of change as Ω_4. The relation $\Omega_2 > \Omega_6 > \Omega_4$ always existed despite the change of Zr^{4+} concentration and the values of Ω_2 were about several times higher than those of Ω_4 and Ω_6. This could be explained with consideration of the peculiarity of the hypersensitive transition $^6H_{15/2} \rightarrow {}^6F_{11/2} + {}^6F_{9/2}$ in absorption spectra. According to the hypersensitive mechanism [42] and "ligand polarization" theory [43] developed by Judd and Mason respectively, the hypersensitive transition arose with the "pseudo-quadrupole" transition, which originated from the asymmetry of ligand environment and local asymmetry of rare-earth ions. Specific types of site symmetry of rare earth ions were required for hypersensitive transitions. Besides, the parameter Ω_2 was rather sensitive to the asymmetry of ligand environment. The Dy^{3+} in octahedral sites in CLN exhibited *C3* or *C1* site symmetry only [44], which are of the right symmetry to excite quadrupole transitions. The exceptionally large oscillator strength of the transition $^6H_{15/2} \rightarrow {}^6H_{9/2} + {}^6F_{11/2}$ in Table 1 clearly indicated the arising of the hypersensitive transition phenomenon [45]. In view of the above, Ω_2 of Zr-2 which is significantly lower indicated that the hypersensitive transition $^6H_{15/2} \rightarrow {}^6F_{11/2} + {}^6F_{9/2}$ was weakened. The central positive ions in oxygen octahedral formed an alternating sequence Li^+-Dy^{3+}-Li^+, Nb_{Li}^{4+}-Dy^{3+}-Li^+ (Dy^{3+} at Nb^{5+} site) or Nb^{5+}-Dy^{3+}- Nb^{5+} (Dy^{3+} at Li^+ site) in Dy:CLN. The sequence Nb_{Li}^{4+}-Dy^{3+}-Li^+ would be aligned in a new way Zr_{Li}^{3+}-Dy^{3+}-Li^+ when the Zr^{4+} was co-doped. As discussed in section 4.1, polarization ability of O^{2-} increased with central ions of higher polarizability ($Li^+ < Zr^{4+} < Nb^{5+}$). It was obvious that the oxygen octahedral environment of Dy^{3+} showed higher symmetry when Nb_{Li}^{4+}-Dy^{3+}-Li^+ transformed to Zr_{Li}^{3+}-Dy^{3+}-Li^+. So, when all the Nb_{Li}^{4+} ions were removed at threshold concentration of Zr^{4+}, the highest symmetry occurred in the crystal field, resulting in the changed covalent chemical bonding and the lowest hypersensitive transition probability. The similar decrease of Ω_2 was also observed in the Dy^{3+} and Zn^{2+} (6mol%) co-doped $LiNbO_3$ crystal [46]. At the exceeding Zr^{3+} concentration, the transformation from Li^+-Dy^{3+}-Li^+ to Zr_{Li}^{3+}-Dy^{3+}-Li^+ dominated and the value of Ω_2 increased, improving the hypersensitive transition probability, which was beneficial for the spectral absorption.

Table 3. Transition probabilities, fluorescence branching ratios and radiant lifetimes of the excited level $^4F_{9/2}$ in Zr:Dy:CLN crystals.

Transition		**Zr-0**		**Zr-1**		**Zr-2**		**Zr-3**	
$^4F_{9/2}$ →	λ_{em} (nm)	*A* (S^{-1})	*β* (%)	*A* (S^{-1})	*β* (%)	*A* (S^{-1})	*β* (%)	*A* (S^{-1})	*β* (%)
$^6F_{5/2}$	1156	21.23	0.57	21.27	0.57	19.37	0.56	20.81	0.57
$^6F_{7/2}$	992	76.37	2.03	76.06	2.04	74.23	2.13	75.14	2.07
$^6H_{5/2}$	918	9.52	0.25	9.59	0.26	7.96	0.23	8.44	0.23
$^6H_{7/2}$	836	56.01	1.49	55.54	1.49	49.70	1.43	52.03	1.43
$^6F_{9/2}$	831	264.34	7.04	263.82	7.09	259.07	7.44	261.87	7.20
$^6F_{11/2}$	748	109.33	2.91	109.05	2.93	102.27	2.94	106.48	2.93
$^6H_{9/2}$	747	54.91	1.46	54.49	1.46	49.79	1.43	52.64	1.45
$^6H_{11/2}$	661	220.23	5.87	219.70	5.91	201.60	5.79	215.11	5.92
$^6H_{13/2}$	576	2251.80	59.97	2241.04	60.25	2075.79	59.62	2187.39	60.17
$^6H_{15/2}$	486	691.06	18.40	669.05	17.99	641.93	18.44	655.28	18.03
		$\tau = 266.33\mu s$		$\tau = 268.84\mu s$		$\tau = 287.22\mu s$		$\tau = 275.09\mu s$	

Transition probabilities, fluorescence branching ratios and radiant lifetime of $^4F_{9/2}$ were figured out with the corresponding oscillator strength parameters by Eq. (6)-(8). These results were tabulated in Table 3. The fluorescence branching ratio of the transition $^4F_{9/2} \rightarrow {}^6H_{15/2}$ (blue fluorescence) increased, while the branching ration of the transition $^4F_{9/2} \rightarrow {}^6H_{13/2}$ (yellow fluorescence) decreased at threshold concentration of Zr^{4+}. These results of fluorescence branching ratios showed a negative correlation between the yellow fluorescence branching ratio and symmetry.

For efficient laser emission, integrated emission cross-section σ_i ($\sigma_i = \sum\left(J \to J'\right) = \lambda^2 A_{JJ'} \big/ (8\pi c n^2)$) is supposed to be greater than 10^{-18} cm [47]. The integrated emission cross-section σ_i of transition from $^4F_{9/2}$ to $^6H_{13/2}$ in Zr-3 was determined to be 1.81 × 10^{-18} cm, while the value of Zr-2 was 1.72 × 10^{-18} cm. Since optical damage resistance dramatically increased only when threshold concentration of Zr^{4+} was reached or exceeded [26], from the results above, only the transition from $^4F_{9/2}$ to $^6H_{13/2}$ of Zr-3 could realize laser operation with high optical damage resistance.

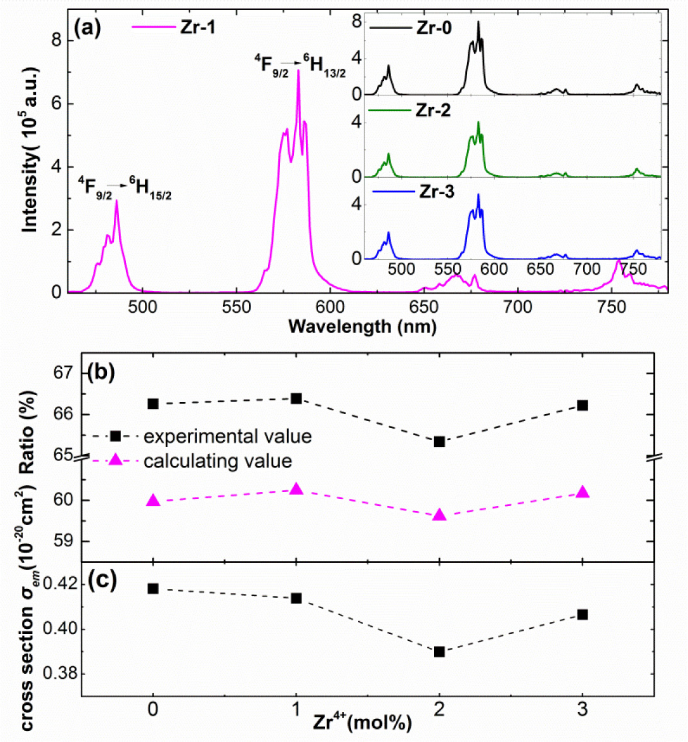

Fig. 5. (a) Fluorescence spectra of Zr:Dy:CLN wafers at room temperature under 450nm excitation. (b) The experimental and calculated fluorescence branching ratios of the transition $^4F_{9/2} \to {}^6H_{13/2}$. (c) The maximum stimulated emission cross sections σ_{em} corresponding to the transition $^4F_{9/2} \to {}^6H_{13/2}$ of Zr:Dy:CLN crystals.

Except for the absorption band centered at 806nm, the absorption band at 450nm related to the transition from $^6H_{15/2}$ to $^4I_{15/2}$ was suitable for optical pumping, especially when the commercialization of blue laser diodes offered convenient access to 450nm pump sources. The fluorescence spectra were recorded under 450nm excitation and displayed in Fig. 5(a). We neglected the weak fluorescence bands in infrared region and evaluated the experimental fluorescence ratios. The experimental and calculated fluorescence ratios of transition $^4F_{9/2} \to {}^6H_{13/2}$ were plotted in Fig. 5(b). The experimental fluorescence ratios were higher than those determined by Judd-Ofelt theory, which could be partly explained with the disregard of infrared fluorescence bands. The ratios β_{exp} decreased at threshold concentration and then increased at exceeding concentration, consistently with the Judd-Ofelt theory analysis. The stimulated emission cross sections σ_{em} were determined by the formula: $\sigma_{em} = \lambda^5 \beta I(\lambda) \big/ (8\pi c n^2 \tau \int \lambda I(\lambda) d\lambda)$, where $I(\lambda)$ is the fluorescence intensity. The dependence on Zr^{4+} concentration of the maximum emission cross sections $\sigma_{em}(10^{-20}cm^2)$ of the transition $^4F_{9/2}\rightarrow{}^6H_{13/2}$ was showed in Fig. 5(c). As shown, the Zr^{4+}, which we co-doped in Dy:CLN crystals to suppress optical damage, had a negative impact on the stimulated emission cross-section at threshold concentration. The negative impact on stimulated emission cross-section was significantly reduced at exceeding concentration of Zr^{4+}. The fluorescence decay curves corresponding to the $^4F_{9/2} \rightarrow {}^6H_{13/2}$ transition of Zr:Dy:CLN crystals were showed in Fig. 6. By single exponential fitting, fluorescence lifetimes were found to be 192.37μs, 196.13μs, 197.81μs and 195.41μs with increasing of Zr^{4+} concentration. The corresponding R-Square was 0.997, 0.998, 0.998 or 0.997 respectively. Doping with Zr^{4+} induced a small increase to lifetime until reaching threshold concentration. The fluorescence quantum efficiency ($\eta = \tau_f/\tau$) was 68.87% and 71.04% for Zr-2 and Zr-3 respectively. This result also showed the excessive doping of Zr^{4+} was necessary.

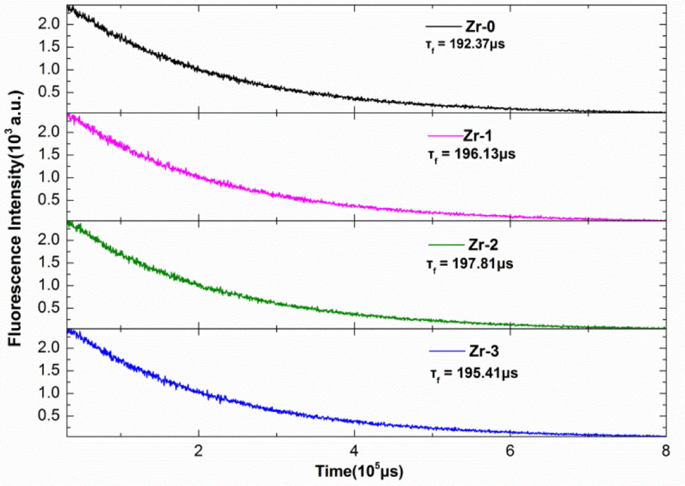

Fig. 6. The fluorescence decay curves of the $^4F_{9/2} \rightarrow {}^6H_{13/2}$ transition in Zr:Dy:CLN crystals.

5. Conclusion

Zr:Dy:CLN single crystals with the fixed concentration of Dy^{3+}(1mol%) and varied concentrations of Zr^{4+} (0, 1, 2, 3mol%) have been grown by the Czochralski technique. The XRD patterns and UV absorption spectra of Zr:Dy:CLN crystals have been recorded. According to the analysis on location of Zr^{4+} and shift of absorption edge position, Nb_{Li}^{4+} had been replaced completely and the number of Li vacancies reached its minimum at threshold concentration (2mol% Zr^{4+}). Based on the UV-Vis-NIR absorption spectra and fluorescence spectra, systematic Judd-Ofelt theory analysis has been carried out. The oscillator strength parameters, fluorescence branching ratios and radiant lifetimes of $^4F_{9/2}$ have been determined and stimulated emission cross sections of transition $^4F_{9/2}\rightarrow{}^6H_{13/2}$ have been evaluated. It turned out that the defects, resulting from Li-deficiency or exceeding Zr^{4+}-doping, would improve the hypersensitive transition probability of $^6H_{15/2}\rightarrow{}^6F_{11/2} + {}^6F_{9/2}$ and have a great impact on Ω_2 .A negative correlation between the yellow fluorescence branching ratio and the symmetry in crystal field was also observed. The concentration of Zr^{4+} was found to have little influence on fluorescence lifetime. These results above suggested that Zr:Dy:CLN wafers can be a candidate material for yellow laser and this work is considered to be promotive for understanding the impact of optical damage resistant ion Zr^{4+} on optical properties of Dy^{3+} doped materials.

Funding

National Natural Science Foundation of China (NSFC) (Nos. 11372361, 11302268, 11232015, 11472321, 11572355); Fundamental Research Funds for the Central Universities; and the Doctoral Program of Higher Education of China (20130171130003).

113.108.133.56 {ts '2017-01-13 02:20:22'}